Available online at www.sciencedirect.com

ScienceDirect

Ciência & Tecnologia dos Materiais 26 (2014) 96–101

Ciência & Tecnologia dos MATERIAIS

http://ees.elsevier.com/ctmat

Special Issue on Biomaterials

# Evaluation of mode I fracture toughness of cortical bone tissue in the RL crack propagation system

F.A.M. Pereira [a], M.F.S.F. de Moura[b,*], N. Dourado[a], J.J.L. Morais[a], M.I.R. Dias[c]

[a] *CITAB/UTAD, Departamento de Engenharias, Quinta de Prados, 5001-801 Vila Real, Portugal*
[b] *Faculdade de Engenharia da Universidade do Porto, Departamento de Engenharia Mecânica, Rua Dr. Roberto Frias, 4200-465 Porto, Portugal*
[c] *UTAD, Departamento de Ciências Veterinárias, Quinta de Prados, 5001-801 Vila Real, Portugal*

**Abstract**

In this work the mode I fracture properties of bone tissue were determined for the RL propagation system. With this aim, Double Cantilever Beam (DCB) fracture tests were performed using specimens of cortical bone tissue harvested from bovine femurs with an age of approximately 8 months. In order to overcome the difficulty associated to the monitoring of crack length during propagation in the course of the test, the CBBM (Compliance Based Beam Method) was used. This method is based on beam theory and experimental specimen compliance, thus allowing the attainment of an equivalent crack length during the test. The results obtained reveal the existence of a plateau on the Resistance-curve, thus making possible to estimate with accuracy the critical strain energy release rate.



*Keywords:* bone; fracture; mode I; double cantilever beam test.

## 1. Introduction

Cortical bone tissue is a composite material with a complex hierarchical, heterogeneous and anisotropic structure. [1]. Besides, it is a living material whose composition and structure alter as a function of mechanical and physiologic environment. Bone is initially formed by primary or plexiform tissue which is gradually replaced by secondary or osteonal tissue. The primary tissue is constituted by collagen fibres disposed in several directions without any defined organization and with minor quantity of minerals [2]. The secondary or osteonal tissue has primary and secondary Havers systems [3]. The primary Havers systems form in the immature skeletal when the growing occurs in parallel to bone longitudinal axis. Collagen fibres randomly disposed between those systems form the well-known trabecular bone tissue. The secondary Havers systems form during organism all life, whilst bone tissue deposition and remodelling take place, being constituted by concentric rings of lamellar bone tissue. The secondary Havers systems are surrounded by interstitial lamellar systems, not b trabecular bone tissue typical of primary Havers systems.

In some published works [4] fracture properties are presented without identification of the fracture propagation system but only the crack propagation direction. This approach is justified by the assumption that bone tissue behaves like an isotropic material in the transverse plane [5]. However, this isotropy is dependent on age, species and type of bone analysed. When young bovine bone of species characterized by quick growth is used, the cortical bone tissue behaves

* Corresponding author.
*E-mail address*: mfmoura@fe.up.pt (M.F.S.F. de Moura)


http://dx.doi.org/10.1016/j.ctmat.2015.03.008

like an orthotropic material owing to presence of plexiform tissue [6], with three directions: L (longitudinal), T (Transversal) and R (Radial). This means that presented properties can only be valid for crack growth in the longitudinal direction, since in the any other direction the fracture properties depend on the propagation system.

The Linear Elastic Fracture Mechanics (LEFM) presents limitations concerning fracture characterization of bone tissue. In fact, fracture of cortical bone tissue is characterized by several toughening mechanisms, e.g., micro-cracking, crack deflection and fibre-bridging [7-11] which result from the composition and bone microstructure. These damaging mechanisms are responsible for a resistance curve on the fracture behaviour of this material [12-14]. This aspect makes the LEFM inexact for this material [15-17]. As a result, several authors have been applying cohesive zone models (CZM) to simulate crack initiation and growth in the cortical bone tissue [16, 18-21]. CZM linked with solid finite elements permit the analysis of several factors inherent to fracture of cortical bone tissue.

Several tests have been used to determine the fracture properties of cortical bone tissue: *Compact Tension* [7], *Chevron-Notched Beam* [22], *Chevron-Notched Tension* [23], *Compact Sandwich Tension* [24] and *Single Notched Beam* [14, 24]. Recently, Morais et al. [20] successfully used a miniaturized version of *Double Cantilever Beam* (DCB) test on the fracture characterization of cortical bovine bone in the TL crack propagation system, which presents several advantages as is the case of allowing the application of beam theory. This aspect makes rendering the development and use of an equivalent crack length based data reduction scheme that simplifies markedly the experiment tests. The DCB tests also provides a stable crack growth and does not constrain the natural formation and propagation of the Fracture Process Zone (FPZ). The authors have concluded that the miniaturized version of DCB test is adequate for bone fracture characterization under mode I loading in the no TL crack propagation system.

In this work, the adequacy of the miniaturized version of DCB test and of the equivalent crack length based data reduction scheme is evaluated for bone fracture characterization under mode I loading in the other crack propagation system (RL), where the limitations related with specimen dimensions are higher than the ones verified for TL system. Experimental tests were performed and the corresponding material resistance curves under mode I loading were obtained. The procedure was numerically validated by finite element analysis including cohesive zone modelling.

## 2. Data reduction scheme

The specimen used in the test was a miniaturized version of the one used in classical DCB tests. To determine the critical strain energy release rate an equivalent crack length based data reduction scheme, known as CBBM (*Compliance Based Beam Method*) [25], was used. The method is based on Timoshenko beam theory and Castigliano theorem to get the relation between specimen compliance ($C$) and crack length ($a$)

$$C = \frac{8a^3}{E_{\mathrm{L}}Bh^3} + \frac{12a}{5BhG_{\mathrm{LR}}} \tag{1}$$

where $E_{\mathrm{L}}$ is the longitudinal elastic modulus, $G_{\mathrm{LR}}$ the shear modulus in the LR plane (bending plane), $B$ the width and $2h$ the specimen thickness. In order to include root rotation and stress concentration effects at the crack tip, an effective modulus $E_{\mathrm{f}}$ can be determined from Equation (1), considering the initials compliance ($C_0$) and crack length ($a_0$), and using the crack length correction $\Delta$ proposed by Williams [20],

$$E_{\mathrm{f}} = \left( C_0 - \frac{12(a_0 + h\Delta)}{5BhG_{\mathrm{LR}}} \right)^{-1} \frac{8(a_0 + h\Delta)^3}{Bh^3} \tag{2}$$

where

$$\Delta = \sqrt{\frac{E_{\mathrm{f}}}{11G_{\mathrm{LR}}} \left[ 3 - 2\left( \frac{\Gamma}{1+\Gamma} \right) \right]^2}$$

$$\Gamma = 1.18 \frac{\sqrt{E_{\mathrm{f}} E_{\mathrm{R}}}}{G_{\mathrm{LR}}} \tag{3}$$

During propagation, Equation (1) is valid replacing $E_{\mathrm{L}}$ by $E_{\mathrm{f}}$, and the actual crack length $a$ by the equivalent crack length $a_{\mathrm{eq}}$,

$$a_{\mathrm{eq}} = a + h\Delta + \Delta a_{\mathrm{ZPF}} \tag{4}$$

yielding

$$C = \frac{8a_{\mathrm{eq}}^3}{E_{\mathrm{f}}Bh^3} + \frac{12a_{\mathrm{eq}}}{5BhG_{\mathrm{LR}}} \tag{5}$$

The term $\Delta a_{\mathrm{ZPF}}$ in Equation (4) was introduced to include the effect of FPZ development occurring at the crack tip during propagation. This phenomenon is

responsible by non-linear behaviour observed in the load-displacement curve before the peak load is attained. Combining the Irwin-Kies relation,

$$G = \frac{P^2}{2B}\frac{dC}{da} \tag{6}$$

with equation (5) leads to,

$$G_{\mathrm{I}} = \frac{6P^2}{B^2 h}\left(\frac{2a_{\mathrm{eq}}^2}{E_{\mathrm{f}} h^2} + \frac{1}{5G_{\mathrm{LR}}}\right) \tag{7}$$

In the course of a fracture test in cortical bone tissue it is not possible to evaluate with rigour the crack length $a$, neither the FPZ extension, $\Delta a_{\mathrm{ZPF}}$ (Equation 4). However, from the initial specimen compliance ($C_0$) and effective elastic modulus $E_{\mathrm{f}}$ (Equations 2 and 3), it is possible to estimate the current compliance $(C = \delta/P)$ and the equivalent crack length $a_{\mathrm{eq}}$ (Equation 5) for each point of $P$-$\delta$ curve. The corresponding evaluation of strain energy release rate ($G_{\mathrm{I}}$), through application of Equation (7), permits to determine the *Resistance-curve* (or *R*-curve), i.e. the relation $G_{\mathrm{I}} = f(a_{\mathrm{eq}})$.

## 3. Experimental

Bone specimens were harvested from fresh bovine femora (Figure 1) of young animals (nearly 8 months) within one day post-mortem period and being preserved in gauzes soaked in physiological saline at −20 ◦C. Specimens were cut from the mid-diaphysis following the anatomic orientations illustrated in Figure 2.

Fig. 1. Bovine femur – detachment of a slice of cortical bone tissue in the diaphysis region.

During milling operations, bone tissue was continuously kept hydrated with physiological saline solution at room temperature (25 ºC). In the course of the cutting operations, specimens were submitted to continuous water irrigation to avoid dehydration and temperature rise. Bone was maintained frozen prior and in between machining operations, being thawed soaked in gauzes at room temperature. Mechanical tests were performed at room temperature (≈25 ◦C) on specimens moisturized with physiological saline. The initial crack length $a_0$ was obtained in two steps. An initial notch was introduced with a circular saw (0.3 mm width), from which the pre-crack was induced using a sharp blade. A testing machine (MicroTester 5848 of INSTRON) was used in this operation. The blade is submitted to a displacement of 0.015 mm with a velocity of 100 mm/min leading to pre-crack execution in a controlled way.

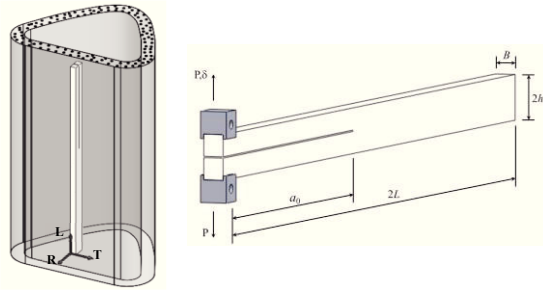


Fig. 2. Schematic representation of DCB specimen.

The DCB tests were performed in the MicroTester 5848 da INSTRON testing machine with a load cell of 2 kN, considering displacement control and a loading velocity of 0.5 mm/min (Figure 3). After the tests, a slice was removed from each specimen to be observed by optical microscopy.

Fig. 3. Photography of a DCB test on bovine bone.

## 4. Numerical analysis

### *4.1. Numerical model*

A preliminary numerical validation of the proposed data reduction scheme (CBBM method) was performed (Figure 4). The elastic and fracture properties used in this procedure are listed in Table 1. The fracture energy is the fundamental parameter of this procedure since it is used as an input parameter ($G_{\mathrm{Ic\ inp}}$) in the cohesive

model. The average value issuing from experimental tests ($G_{Icinp}$=0.86 N/mm in Table 2) was considered. The numerical load-displacement curves resulting from simulations were used to obtain the *R*-curves following the CBBM. The resultant $G_{Ic}$, measured at the plateau of the *R*-curve, is compared with the $G_{Icinp}$.

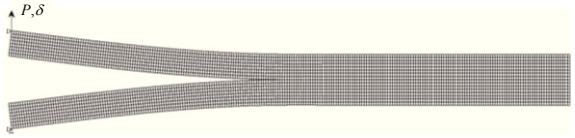


Fig. 4. Mesh and boundary conditions used in the numerical simulation of the DCB test.

The validation procedure consists on the verification whether the proposed data reduction scheme is able to produce an *R*-curve which tends to a horizontal asymptote converging with $G_{Ic\ inp}$ introduced in the numerical model.

Table 1. Bone elastic and fracture properties used in the numerical model

| Elastic properties | | | | Fracture properties | |
|---|---|---|---|---|---|
| $E_L$ (GPa) | $E_R$ (GPa) | $\nu_{LR}$ | $G_{LR}$ (GPa) | $G_{Ic}$ (N/mm) | $X_T$ (MPa) |
| 12,2[4] | 5,9 [2] | 0,41[1] | 5,1 [1] | 0,86 [3] | 32 [5] |

[1] Taken from [20].
[2] Taken from [31].
[3] Experimentally measured.
[4] Obtained from numerical-experimental fitting (inverse method).
[5] Normal strength obtained from numerical-experimental fitting (inverse method).

### *4.2. Cohesive model*

Two-dimensional interface finite elements with 6 nodes compatible with 8-node plane stress solid element were used to simulate damage onset and propagation. The pure mode cohesive model is based on a relationship between stress and relative displacement ($\sigma_i$ versus $w_i$ with $i$ = I, II) as shown in Figure 5. This law requires the definition of two independent parameters (local strength $\sigma_{u,i}$ and critical strain energy release rate $G_{ic}$) that can be measured experimentally. The relative displacement $w_{o,i}$ is calculated as a function of local strength $\sigma_{u,i}$ (assumed equal to $X_T$ –Table 1) and the interfacial stiffness. The optimum value of this parameter corresponds to the highest value that does not induce numerical problems. The majority of structural problems are well solved considering values of interfacial stiffness ranging between $10^6$ a $10^8$ N/m$^3$ [26].

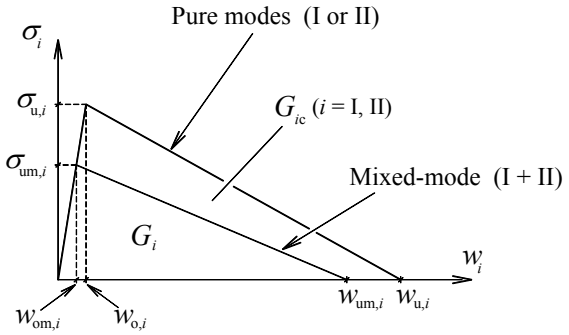


Fig. 5. Pure and mixed-mode I+II damage models.

The mixed-mode (I+II) damage law is an extension of the pure mode one and is based on a quadratic stress criterion to simulate damage onset

$$\left(\frac{\sigma_I}{\sigma_{u,I}}\right)^2+\left(\frac{\sigma_{II}}{\sigma_{u,II}}\right)^2=1 \quad \text{if } \sigma_I \geq 0$$
$$\sigma_{II}=\sigma_{u,II} \quad \text{if } \sigma_I < 0 \tag{8}$$

It is assumed that compressive stresses do not contribute to damage. Damage propagation is simulated by the linear energetic criterion,

$$\frac{G_I}{G_{Ic}}+\frac{G_{II}}{G_{IIc}}=1 \tag{9}$$

The fracture properties of mode II were obtained in [27]. It should be noted that pure mode I loading is a particular case of a mixed-mode one where mode II becomes negligible.

## 5. Results and Discussion

The images obtained by optical microscopy were used to characterize the microstructure of tested bone. In all specimens plexiform and osteonal bone tissues were identified (Figure 6). In this figure it is also possible to observe differences in the microstructure of young cortical bovine bone between radial and tangential directions which explains the orthotropic behaviour.
Figure 7a shows a typical experimental load-displacement curve and Figure 7b the corresponding *R*-curve obtained from CBBM.

The increase of critical strain energy release rate observed in the ascending part of the *R*-curve reflects the development of the fracture process zone (FPZ) and corresponds to the non-linear part of load-displacement curve preceding the peak load.

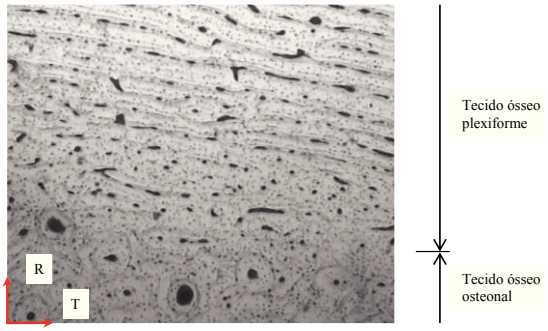


Fig. 6. Microstructure of young cortical bone tissue.

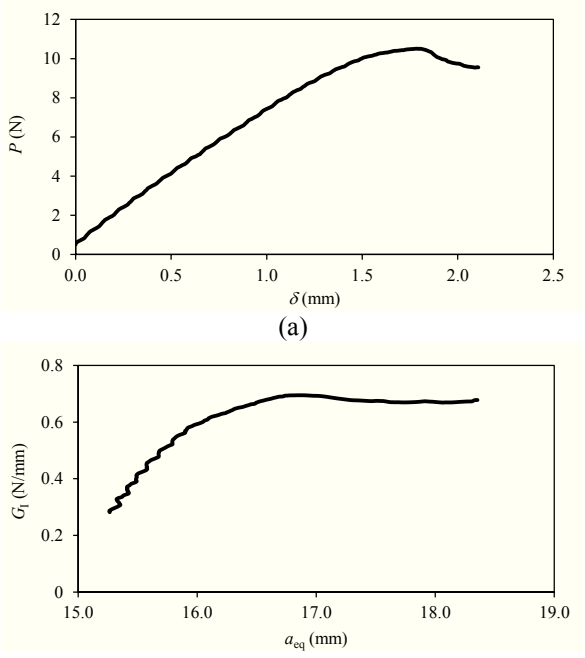


Fig. 7. Typical experimental curves: (a) Load-displacement and (b) *R*-curve.

This phenomenon induces material softening leading to a gradual decrease of stiffness up to crack onset. In the *R*-curve an increase of equivalent crack length (approximately 1.0 mm) can be observed as a result of FPZ development. The existence of a plateau allows to define the critical strain energy release rate ($G_{Ic}$). In fact, at the beginning of the plateau the critical dimension of the FPZ is achieved and maintains constant in the course of crack propagation, since the conditions of self-similar crack growth are satisfied for a given crack extent.

Table 2 presents the average value of fracture energy considering ten tests. It should be noted that the high coefficient of variation (i.e., 22.4%) results from variability of a natural material as observed in other works [20,24,28,29]. The average value obtained in propagation system RL (i.e., 0.86 N/mm) is markedly lower than the one obtained previously by Morais et al. [20] for the TL crack propagation system (i.e., $G_{Ic}$=1.91 N/mm). Wang and Agrawal [30] have already observed values noticeably lower for the RL crack propagation system relative to TL one.

Table 2. Experimental results (ten tests) of fracture energy under mode I loading for TL crack propagation system [20].

| | $G_{Ic}$ (RL) (N/mm) | $G_{Ic}$ (TL) (N/mm) |
|---|---|---|
| Average | 0.86 | 1.91 |
| CV (%) | 22.4 | 15.5 |

A numerical analysis of the DCB test considering the cohesive model shown in Figure 5 and the properties listed in Table 1 was performed to validate the procedure to measure the $G_{Ic}$ of bone. Figure 8(a) compares the numerical and experimental $P$-$\delta$ curves for one specimen. In the numerical simulation the value of $G_{Ic\ inp}$ was taken from the plateau of the *R*-curve (Figure 8b).

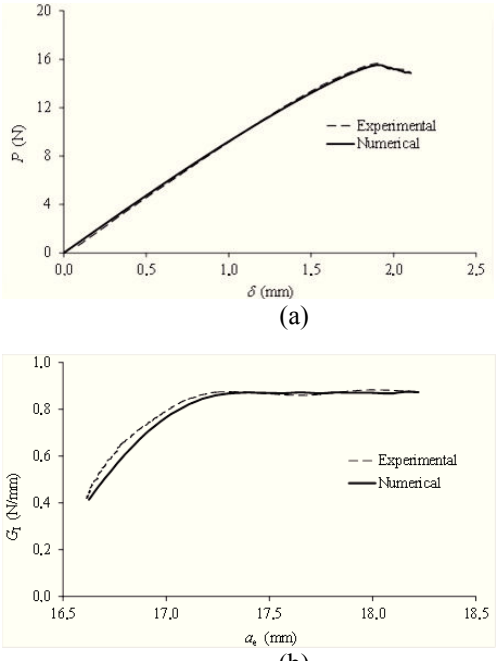


Fig. 8. Comparison between numerical and experimental: (a) $P$-$\delta$ curves and (b) *R*-curves.

It can be observed that numerical $P$-$\delta$ curve presents an excellent agreement with the experimental one. Additionally, the $G_{Ic\ inp}$ value is well captured in the plateau of the *R*-curve, which demonstrates the adequacy of the proposed data reduction scheme.

## 6. Conclusions

In this work, fracture behaviour of cortical bone tissue of young bovine under mode I loading in the RL crack propagation system was performed. In order to determine the critical strain energy release rate a miniaturized version of the DCB test was used. The main advantage of this test relative to other fracture tests is the easy application of data reduction methods based on beam theory analysis. In this context a data reduction scheme (CBBM) based on specimen compliance, equivalent crack length and Timoshenko beam theory was developed and applied to obtain the *R*-curves without requiring crack length monitoring during the test. A numerical validation was performed by means of a finite element analysis using cohesive elements. The optical microscopy allowed to identify several types of cortical bone revealing a clear material orthotropic behaviour. This aspect reveals the significance of fracture characterization as a function of plane of propagation, specifically in the young cortical bone tissue derived from animals of quick growth.

The results obtained in this work prove the adequacy of this test for the fracture characterization of cortical bone tissue under mode I loading in the RL crack propagation system.

## Aknowledgements

The authors acknowledge the Portuguese Foundation for Science and Technology (FCT) for the conceded financial support through the research project PTDC/EME-PME/119093/2010. The first author acknowledges the FCT for the conceded financial support through the PhD grant SFRH/BD/80046/2011.

## References

[1] J.-Y. Rho, L. Kuhn-Spearing, P. Zioupos, *Med. Eng. Phys.* **20**, 92-102 (1998).
[2] L.C. Junqueira, J. Carneiro "Histologia básica". Guanabara Roogan, 7ª ed,, 611-018, 1990.
[3] M. Dias, L. Costa, C. Viegas, H. Alves, M. Pires "O Tecido Ósseo Biologia da Cicatrização". Série Didáctica. Ciências Aplicadas; 280, Universidade de Trás-os-Montes e Alto Douro, Vila Real, 2005.
[4] M. Doblaré, J.M. García, M.J. Gómez, *Eng. Fract. Mech*. **71,** 1809-1840 (2004).
[5] D.T. Reilly, A.H. Burstein, *J. Biomech.* **8**, 393-405 (1975).
[6] J.D. Currey "Bones: structure and mechanics". Princeton University Press, Princeton, 2002.
[7] A. Bingbing, L. Yang, A. Dwayne, Z. Dongsheng, *J. Mech. Behav. Biomed*. **4**, 983-992 (2011).
[8] P.Zioupos, *Mat. Sci. Eng. C-Mater*. **6**, 33-40 (1998).
[9] D. Vashishth, K.E. Tanner, W. Bonfield, *J. Biomech.* **33**, 1169-1174 (2000).
[10] Y.N. Yeni, T.L. Norman, *J. Biomed. Mater. Res. B*, **51**; 504-509 (2000).
[11] R.K. Nalla, J.H. Kinney, R.O. Ritchie, *Nat. Mater.* **2**, 164-168 (2003).
[12] C.L. Malik, S.M. Stover R.B. Martin, J.C. Gibeling, *J Biomech.* **36**, 191-198 (2003).
[13] D.Vashishth, *J. Biomech*. **37**, 943-946 (2004)
[14] K.J. Koester, H.D. Barth, R.O. Ritchie, *J. Mech. Behav. Biomed*. **4**, 1504-1513 (2011).
[15] P. Lucksanasombool, W.A.J. Higgs, R.J.E.D. Higgs, M.V. Swain, *Biomater*. **22**, 3127-3132 (2001).
[16] A. Ural, D.Vashishth, *J. Biomech*. **39**, 2974-2982 (2006).
[17] R.O. Ritchie, K.J. Koester, S. Ionova, W. Yao N.E. Lane, J.W. Ager, *Bone*. **43**, 798-812 (2008).
[18] Q.D. Yang, B.N. Cox, R.K. Nalla, R.O. Ritchie, *Bone* **38**, 878-887. (2006).
[19] B.N. Cox, Q. Yang, *Eng. Fract. Mech*. **74**, 1079-1092 (2007).
[20] J.J.L. Morais, M.F.S.F. de Moura, F.A.M. Pereira J. Xavier, N. Dourado, M.I.R. Dias, J.M.T. Azevedo, *J. Mech. Behav. Biomed*. **3**, 446-453 (2010).
[21] A. Ural, *Proc Eng.* **10**, 2827-2832 (2011).
[22] J. Yan, K.B. Clifton, J.J. Mecholsky, R.L. Reep, *J Biomech*. **39**, 1066-1074 (2006).
[23] R. de Santis, P. Anderson, K.E. Tanner, L. Ambrosio, L. Nicolais, W. Bonfield, G.R. Davis, *J. Mater. Sci-Mater. M.* **11**, 629-636 (2000).
[24] J.B. Phelps, G.B. Hubbard, X. Wang, C.M. Agrawal, *J. Biomed. Mater. Re.s A*, **51**, 735-741 (2000).
[25] F.A.M. Pereira, J.J.L. Morais, M.F.S.F. de Moura, N. Dourado, M.I.R. Dias, *Eng. Fract. Mech.* **96**, 724-736 (2012).
[26] M.F.S.F. de Moura, J.P.M. Gonçalves, A.T. Marques, P.M.S. Tavares de Castro, *J. Comp. Mater.*, **31**, 1462-1479, (1997).
[27] F.A.M. Pereira, J.J.L. Morais, N. Dourado, M.F.S.F. de Moura, M.I.R. Dias, *J. Mech. Behav. Biomed*. **4**, 1764-1773 (2011).
[28] J. McCormack, S. M. Stover, J. C. Gibeling, D. P. Fyhrie, *Bone*, **50**, 1275-1280 (2012).
[29] J. S. Nyman, A. Roy, X. Shen, R. L. Acuna J. H. Tyler, X. Wang, *J. Biomech*. **39**, 931-938 (2006).
[30] X. Wang, C. M. Agrawal. *J. Biomed. Mater. Res.* **33**, 13–21 (1996).
[31] M.E. Szabó, P. J. Thurner. *J. Biomech.* **46**, 2-6 (2013).